Available online at www.sciencedirect.com
SCIENCE DIRECT®
Journal of Power Sources 142 (2005) 313–322
JOURNAL OF POWER SOURCES
www.elsevier.com/locate/jpowsour

Effect of operation conditions on simulated low-earth orbit cycle-life testing of commercial lithium-ion polymer cells

Xianming Wang*, Yoshitsugu Sone, Saburo Kuwajima

Institute of Space Technology and Aeronautics, Japan Aerospace Exploration Agency, Tsukuba Space Center, Sengen 2-1-1, Ibaraki 305-8505, Japan

Received 11 June 2004; accepted 20 October 2004
Available online 15 December 2004

Abstract

Laminated lithium-ion polymer cells with gel electrolytes and laminate-film package are expected to replace the conventional alkaline batteries for space application due to their high energy density and high flexibility in configuration. To facilitate this, we assessed the effect of operation conditions, charge rate and taper voltage, on cycle-life testing of commercial lithium-ion polymer cells by simulating a satellite's LEO operation with 40% DOD profile in this work. So far, 6000 cycles have been completed. A lower charge rate was found to be promising for long-term satellite operation. Impedance analysis disclosed a little change in cell internal impedance with charge rate. This encouraged us to attribute the poor cycling performance at high charge rate to excessive lithium-ion exhaust in electrode surface-film formation due to a longer holding duration at taper voltage. The taper voltage was also found to affect charge performance of lithium-ion polymer cells. Good cycling performance, such as the minimum current at the end of the charge and the maximum voltage at the end of the discharge were observed when using taper voltage range from 4.05 to 4.10 V. Theoretical analysis deduced that low current at the end of the charge correlated to (1) a low cell internal impedance and (2) a large slope in the capacity–voltage charge curve measured at a low rate. We further evaluated cell cycling behavior at a low rate and indeed observed the largest slope of capacity–voltage charge curve at voltages ranging from 4.05 to 4.10 V.

Keywords: Lithium-ion polymer cell; Satellite application; Charge rate; Taper voltage; Impedance

1. Introduction

Due to strict constraints on weight and volume of bus components in a satellite, lithium-ion batteries, which have high energy density and high working voltage, have been expected to replace conventional nickel–cadmium (Ni–Cd) and nickel–hydrogen (Ni–H_2) batteries [1–5]. To facilitate this, lithium-ion cells with capacities ranging from 0.6 to 100 Ah are being assessed in real-time by simulating low-Earth-orbit (LEO) or geosynchronous-Earth-orbit (GEO) satellite operation at the Japan Aerospace Exploration Agency (JAXA, former National Space Development Agency of Japan) [6–9]. A few types of these cells have been found to show impressive performance. Their energy densities exceed 100 Wh kg^{-1}, about twice as large as those of Ni–Cd and Ni–H_2 cells. Furthermore, excellent cycle lives exceeding 20,000 cycles in LEO simulation mode have been verified with cell voltages of above 3.5 V at the end of the discharge. The same effort is also devoted by other space organizations [10–14]. The satisfactory on-ground evaluation results have recently encouraged some of these organizations to propose demonstrating the cycling performance of lithium-ion cells in the practical space environment [15–18].

Generally, commercial lithium-ion cells may be divided into the following two types according to their electrolyte states. One type is the common lithium-ion cell with liquid electrolyte. Cell components are contained in a metal case, so this type of lithium-ion cell may be easily made larger and thus suitable for large-capacity satellites. The other type is the lithium-ion polymer cell, which contains polymer support material to form gel electrolytes by incorporat-

* Corresponding author. Tel.: +81 29 868 4247; fax: +81 29 868 5969.
E-mail address: oh.kenmei@jaxa.jp (X. Wang).

0378-7753/$ – see front matter © 2004 Elsevier B.V. All rights reserved.
doi:10.1016/j.jpowsour.2004.10.014

Table 1
Typical specifications of lithium-ion polymer cells evaluated in this work

Sample	Nominal capacity (Ah)	Nominal voltage (V)	Anode and cathode	Cell weight (g)	Dimensions (mm)	Experiment
Cell 1	0.56	3.7	Graphite and $LiCoO_2$	13.37	59, 30, 3.5	Charge rate of 0.5 C
Cell 2				13.40	57, 31, 3.5	
Cell 3				13.36	59, 30, 3.5	Charge rate of 1.0 C
Cell 4				13.34	58, 30, 3.5	
Cell 5				13.39	59, 31, 3.5	Taper voltage effect

ing organic electrolytes. Unlike common lithium-ion cells, lithium-ion polymer cells utilize aluminum laminate-film packages, and thus exhibit the advantages of high energy density and high flexibility in configuration. However, this aluminum laminate-film package may limit the cell only to small sizes due to a difficulty in cell sealing. For this reason, the lithium-ion polymer cell seems to be more promising for small-capacity space applications (e.g., microsatellites, space probes, rovers). Recently, more and more microsatellite projects are being announced all over the world since microsatellite technology appears to provide affordable access to space for low-budget utilizations [19,20]. This makes it necessary to develop lithium-ion polymer cells in order to improve mass and volume efficiencies of the battery system. Nevertheless, development and research on lithium-ion cells for space application have been to date mainly limited in that with liquid-state electrolyte. Little data on lithium-ion polymer cell were reported.

The main objective of this work is to evaluate the applicability of commercial lithium-ion polymer cells for satellite energy storage applications. To realize space application of a lithium-ion polymer cell, some particular operation conditions and environments, such as vacuum state, outgas from the polymer components, safety concerns, long cycle-life requirement and short charge and discharge intervals limited strictly by spacecraft orbit, must be considered. Typically, a spacecraft in LEO (within 1000 km from the Earth) periodically experiences about 60 min sunshine and 30 min eclipse [1,6]. This requires that on-board rechargeable cells store necessary power from solar cells at a short interval of 60 min, and generate enough power to meet electrical demands of bus and mission at a very short interval of 30 min. Rechargeable cells must thus exhibit good cycling performance even at high charge and discharge rates. This makes it important to optimize the operation conditions, such as charge rate and taper voltage. For this reason, many rather novel experimental investigations need to be done in order to utilize lithium-ion polymer cells as power sources in space.

In this work, we mainly assessed the effect of charge rate and taper voltage on cycling performance of lithium-ion polymer cells by simulating satellite's LEO operation with a depth of discharge (DOD) of 40%. In order to understand the experiment results, a impedance measurement and a theoretical analysis were conducted to find the factors affecting cell cycling performance.

2. Experimental

2.1. Sample of lithium-ion polymer cell

Table 1 lists typical specifications of lithium-ion polymer cells evaluated in this work. These cells mainly consisted of $LiCoO_2$ cathode, graphite anode, gel electrolyte, and an aluminium laminate-film package. The gel electrolyte was formed by incorporating $LiPF_6$/EC + EMC organic electrolyte into PVdF-based polymer support material, and stuck both laminate package and electrode active materials. This structure maintains the configuration stability of the cell even in a vacuum, and has been found to contribute to good cycling performance results of these cells in a simulated space environment in our previous work [9].

2.2. Charge rate effect

We first used four cells to evaluate the effect of charge rate on cycle-life performance. These cells were set on a thermostatic plate (Toyo Seisakusho, Advantec LV-600) of $19 \pm 1\,^{\circ}C$. Cycle-life testing was performed with a charge–discharge system (Advanced Engineering Services, 2004-C101). Cell voltage and cell temperature were monitored during cycle-life testing.

2.2.1. Cycle-life testing at different charge rates

Cells were tested by simulating satellite's LEO operation with a DOD of 40% under regimens of constant current–constant voltage (CC–CV) charge and constant current (CC) discharge. At the beginning of cycle-life testing, the cells were first precharged with a taper voltage of 4.1 V, a total charge time of 6 h and a charge rate of 0.5 or 1.0 C. In every charge–discharge cycle, the cells were charged with a charge time of 60 min, taper voltage of 4.1 V, charge rate of 0.5 or 1.0 C, and discharged with a discharge time of 30 min, discharge rate of 0.8 C. Cycle-life was judged from the cycle where voltage in the discharge phase dropped to 2.8 V.

2.2.2. Capacity verification during cycling

During cycle-life testing, residual capacity and real capacity of every cell were verified at fixed periods. Residual capacity was measured by directly discharging cells in CC mode with a discharge rate of 0.5 C and a cut-off voltage of 3.1 V after charging the cell under cycle-life-testing conditions. The cell was then charged in CC–CV mode with a

charge rate of 0.5 C, a taper voltage of 4.1 V and a total charge time of 6 h, and discharged at the same discharge condition as that of residual capacity. The capacity obtained here was defined as the real capacity. The difference in residual capacity and real capacity was attributable to much longer charge time in real capacity measurement than in residual capacity measurement, and reflected the capacity fading during cycle-life testing due to cell internal impedance.

2.2.3. Impedance measurement

After every capacity verification, the cell was left in the open-circuit state for at least 1 h to stabilize the cell voltage. We then measured the ac impedance with a frequency ranging from 10 kHz to 0.01 Hz at 5 mV potentiostatic signal amplitude with a Solartron FRA 1255B frequency response analyzer and a Solartron model 1287 electrochemical interface.

2.3. Taper voltage effect

Next, we used one cell to evaluate the taper voltage effect on cycling performance. The electrochemical tests were performed with a charge–discharge battery tester (Kikusui, PFX40W-08) in a thermostatic program incubator (Yamato, IN600) of $20 \pm 1\,^{\circ}C$.

2.3.1. Cycle-life testing with different taper voltage

The cells were tested by simulating satellite LEO operation with a DOD of 40% under the profiles of constant current–constant voltage (CC–CV) charge and constant current (CC) discharge. The cell was charged at a charge rate of 0.5 C, total charge time of 60 min and different taper voltages ranging from 4.2 to 3.9 V with an interval of 50 mV. The cell was discharged with a discharge rate of 0.8 C and a total discharge time of 30 min. The cell was cycled five times at every taper voltage level. Before cycling at every taper voltage, the cell was precharged with the taper time of 2 h and charge rate of 1 C in order to make the cell in the same initial state.

Since the nominal capacity was obtained at a constant taper voltage of 4.2 V, it is necessary to measure the cell capacities at different taper voltages in order to calculate the charge (discharge) current. The cell-capacity at every taper voltage was measured as shown below.

2.3.2. Capacity verification

The cells were charged in CC–CV mode at a rate of 1 C, a taper voltage ranging from 4.2 to 3.9 V with an interval of 50 mV and taper time of 2 h. The cells were discharged in CC mode at a rate of 0.2 C and cut-off voltage of 3.0 V. Here, we measured the current by using the nominal capacity of every cell, which was generally determined by using a taper voltage of 4.2 V. Due to a long charge duration and a small discharge rate, the error come from the current calculated by nominal capacity was enough small and might be neglected.

2.3.3. Charge and discharge at slow rate

To correlate the taper voltage with cycling performance of lithium-ion polymer cells, we further charged and discharged cells slowly to suppress the effect of cell internal impedance. The test conditions were the same as those in capacity measurement except for the charge and discharge rates of 0.1 C, and the fixed taper voltage of 4.2 V.

3. Results and discussion

3.1. Charge rate effect

The nominal capacity of 0.56 Ah was used to calculate the charge and discharge currents of lithium-ion cell in cycle-life testing. As a result, the charge and discharge currents were set to 0.28 A (0.56 A) and 0.45 A, corresponding to 0.5 C (1.0 C) and 0.8 C, respectively.

Generally, current at the end of the charge and voltage at the end of the discharge are two important parameters to compare cycling performance of cells. In order to charge the cell in CC–CV mode in a very short duration, a low current at the end of the charge is desirable. In addition, a high voltage

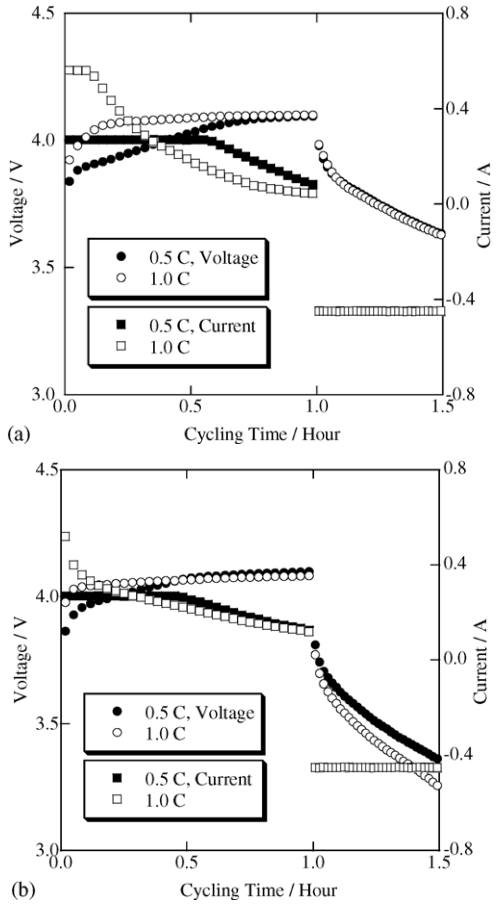

Fig. 1. Charge and discharge curves with different charge rates for lithium-ion polymer cells 1 and 3 at (a) cycle 5 and (b) cycle 4999. Charge rate is indicated in graph.

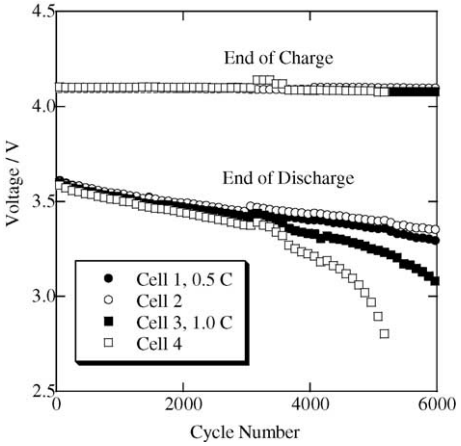

Fig. 2. Voltage trends at the end of the charge and discharge for lithium-ion polymer cells with different charge rates. Lower charge rate was promising for long-term charge–discharge cycling.

at the end of the discharge is needed for long-term satellite operation.

As an example, charge and discharge curves of lithium-ion polymer cells 1 and 3 at different charge rates are shown in Fig. 1. At initial cycles, the high charge rate resulted in a low current at the end of the charge and a similar voltage at the end of the discharge. However, at cycle 4999, the cell charged at high rate exhibited a lower voltage at the end of the discharge than that charged at a low rate.

Fig. 2 shows voltage trends at the end of the charge and discharge. Some 6000 charge–discharge cycles have been completed, corresponding to about 1-year LEO satellite operation. Comparing the voltage at the end of the discharge revealed that the voltage at the end of the discharge with high charge rate became lower than that with low charge rate after 3000 cycles. This indicated that a low charge rate was appropriate for the long-term cycling of lithium-ion polymer cells used for LEO satellites, similar to the result obtained from Fig. 1.

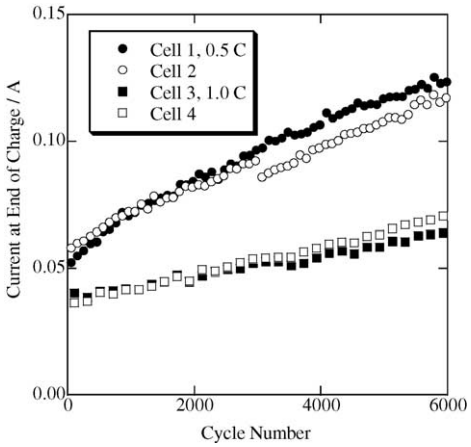

Fig. 3. Current trends at the end of the charge for lithium-ion polymer cells with different charge rates. A bigger current increase at end of charge was observed when using a charge rate of 0.5 C than that of 1.0 C.

As shown in Fig. 1, the cell current diminished with charge time at the taper voltage in the CV phase. This decrease in charge current depends entirely on the cell internal impedance. Fig. 3 indicates the current trend at the end of charge. Overall, the current at the end of the charge increased with cycling regardless of the charge rate, indicating an increase of cell internal impedance. However, a comparison of the current trends at different charge rates revealed that a high charge rate led to a lower current at the end of the charge than that of low charge rate. This demonstrates good charge performance at a high charge rate.

During the cycle-life testing, cell capacities were verified at a fixed period. Fig. 4 shows the changes of residual capacity and real capacity. The difference of residual capacity and real capacity is caused by much longer charge time in real capacity measurement than in residual capacity measurement. Therefore, this difference reflects the capacity loss during cycle-life testing due to cell internal impedance. So far, the capacities have been verified up to 5000 cycles. A high charge rate led to larger capacity fading than that at low charge rate, coinciding well with the result in Fig. 2. After 3000 cycles, a severe capacity fading was observed when using the charge rate of 1.0 C. However, the difference in residual capacity and

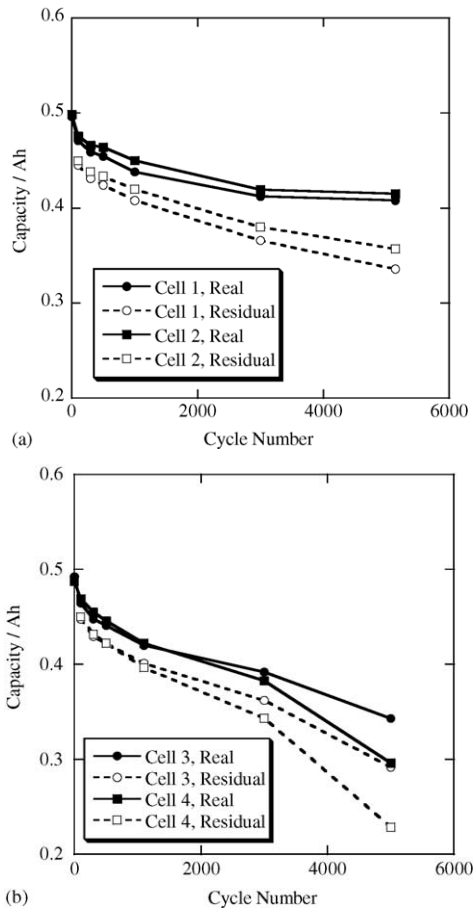

Fig. 4. Fading curves of real capacity and residual capacity for lithium-ion polymer cells at a charge rate of (a) 0.5 C or (b) 1.0 C. A higher charge rate of 1.0 C led to more serious capacity fading.

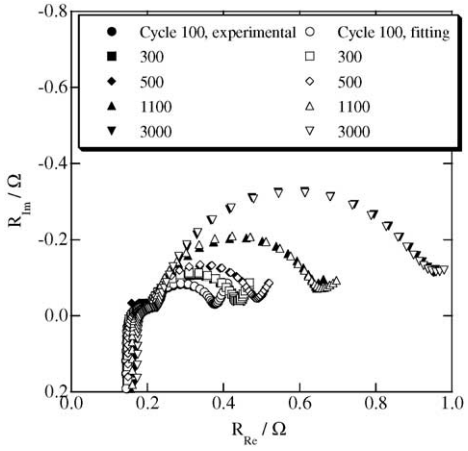

Fig. 5. Nyquist impedance plots of experimental data and fitting results for lithium-ion polymer cell 3 with a charge rate of 1.0 C after capacity measurement. Fitting results agreed well with experimental data. The semicircle in the high-frequency range did not change with cycling, in contrast to semicircle in middle-frequency range.

real capacity was almost independent of the charge rate. This demonstrates that it is difficult to attribute cell-performance degradation only to an increase in the cell internal impedance. It is possible that some other factors cause cell-capacity fading.

In order to identify the capacity fading mechanism, we measured cell impedance after every capacity verification. As an example, Fig. 5 shows impedance spectra of lithium-ion polymer cell 3 for a charge rate of 1.0 C as a function of cycle number. Two separated semicircles may be distinguished in the medium frequency range between 15.8 and 63.1 Hz, dependent on cycle number. In the low-frequency range, a straight line was observed, reflecting lithium-ion diffusion process in electrode active materials represented by well-known 45°-slope Warburg line characteristic of the diffusion. Furthermore, we found that the semicircle in the high-frequency range did not change with cycling, in contrast to the semicircle in the middle-frequency range.

In fact, some groups have investigated impedance responses of lithium-ion cells during storage and cycling by using two-electrode and three-electrode configurations [21–27]. It was commonly acceptable that the contribution to cell impedance from anode appeared only at high frequency, while the impedance at moderate to low-frequency was due to the cathode. By using this knowledge, we deduced from Fig. 5 that the cell impedance was largely dictated by the cathode, rather than the anode or electrolyte. Cell impedance increase with cycling was also mainly due to the cathode contribution. These results coincided well with those reported by other authors [26,27].

In a general sense, the charge and discharge of lithium-ion cell is primarily concerned with the electrode/electrolyte interphase reaction, and lithium-ion diffusion in electrolyte and electrode active materials. Therefore, cell internal impedance may be represented by the equivalent circuit shown in Fig. 6. Here L is the inductance corresponding to rolled electrodes and lead wire, R_e the electrolyte resistance, and C_v the cell-capacity at a given voltage. $R_{a,f}$ and $C_{a,f}$ are resistance and capacitance of the anode surface film, $R_{a,ct}$ is the charge transfer resistance of the anode, $R_{c,f}$ and $C_{c,f}$ are the resistance and capacitance of the cathode surface film, and $R_{c,ct}$ the charge transfer resistance of the cathode. In addition, $C_{a,dl}$ and $C_{c,dl}$ (W_a and W_c), are constant-phase elements, corresponding to double-layer capacitances (lithium-ion diffusion resistances) of the anode and cathode.

Parameter fitting with Zview software was conducted for the experimental data. Some fitting results are shown in Fig. 5. Obviously, these fitting results agreed well with the experimental data. To a certain extent, this confirms the accuracy of above equivalent circuit.

Since phenomena associated with the cathode were major contributors to cell impedance, we concentrate on the cathode charge transfer resistance, $R_{c,ct}$, in the following discussion. Fig. 7 compares $R_{c,ct}$ of every cell for different charge rates. In a common sense, the following cell behavior at a high charge rate may be considered as the primary cause of poor cycling performance. At a high charge rate, the cell was held at the taper voltage for a longer time. As a result, electrolyte may be subjected longer to redox decomposition on the electrode surface, which is generally accompanied by excess lithium-ion exhaust [28–30]. The electrolyte-decomposition products may deposit on electrode surface and form a high-impedance film. From Fig. 7, it may be found that the cathode charge transfer resistances obtained at different charge rates were almost identical at the same cycle. This encouraged us to believe that the excess lithium-ion exhaust, rather than the cell internal impedance, was a main cause of cell-performance degradation at a high charge rate.

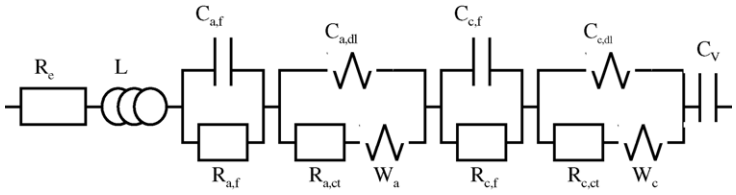

Fig. 6. Equivalent circuit used to fit the impedance spectra of lithium-ion polymer cells obtained in this work. L denotes inductance, R_e electrolyte resistance, and C_v cell-capacity at a given voltage. $R_{a,f}$ and $C_{a,f}$ ($R_{c,f}$ and $C_{c,f}$) are resistance and capacitance of the anode (cathode) surface film; $R_{a,ct}$ ($R_{c,ct}$) charge transfer resistance of anode (cathode). $C_{a,dl}$ ($C_{c,dl}$) and W_a (W_c) are constant-phase elements of anode (cathode).

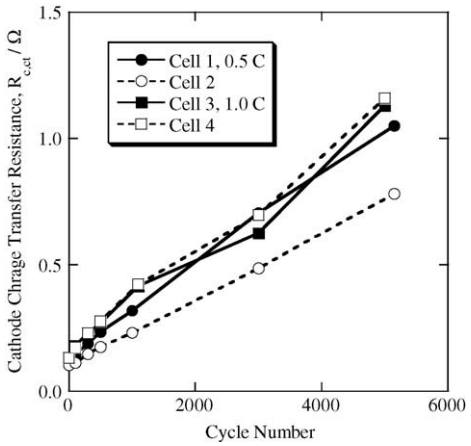

Fig. 7. Charge transfer resistances of cathode, $R_{c,ct}$, as a function of cycle number at a charge rates of (a) 0.5 C or (b) 1.0 C. No significant difference in $R_{c,ct}$ was observed at different charge rates.

The excess lithium-ion exhaust may become serious due to excess cell volume change in a high charge rate [31]. Fig. 8 plots open-circuit voltage as a function of cycle number after capacity verification in Fig. 4. Obviously, open-circuit voltage tended to increase with cycling, indicating more and more residual lithium-ion in anode active material after discharging. These residual lithium ions cannot take part in charge–discharge process again, resulting in cell-performance degradation. As a result, the graphite anode ($LiCoO_2$ cathode) active materials expanded due to lithium-ion excess (lack). The detrimental electrode expansion on the cycling behavior includes both electrode crumbling and excess exhaust of lithium ions due to the formation of solid electrolyte interphase (SEI) on the new electrode surface. Indeed, we have found more residual lithium-ion in a graphite anode experienced about 4000-cycle LEO-simulating cycle-life testing than that of a fresh graphite anode by using NMR analysis in another work.

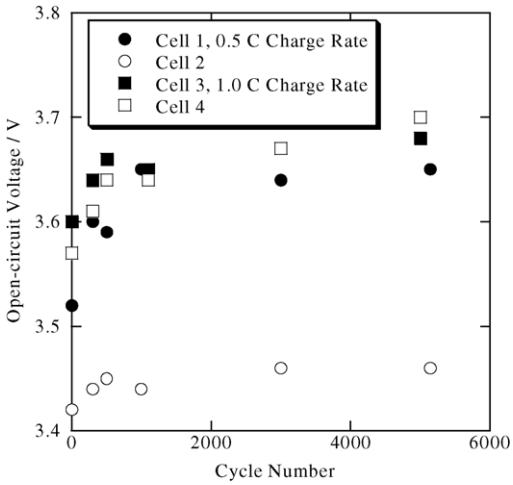

Fig. 8. Open-circuit voltage after capacity verification as a function of cycle number for lithium-ion polymer cells with different charge rates. Open-circuit voltage tended to increase with cycling.

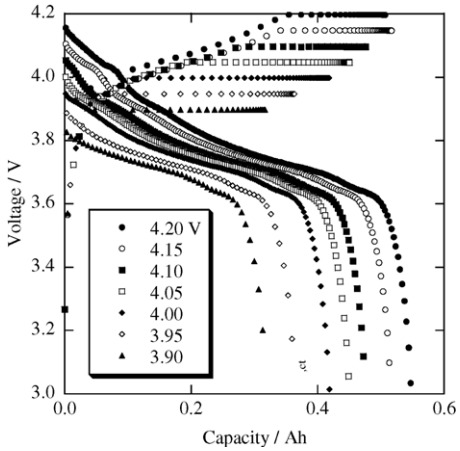

Fig. 9. Charge and discharge curves of the lithium-ion polymer cell 5 as a function of taper voltage. Capacity decreased with decreasing taper voltage.

3.2. Taper voltage effect

Here, we first verified the capacity to calculate the charge and discharge currents at different taper voltages. Fig. 9 shows charge and discharge profiles of the lithium-ion polymer cell. Strictly speaking, charge and discharge currents should be calculated by using the actual capacity at different taper voltages, rather than the nominal capacity here. Nevertheless, since we used a low discharge rate of 0.2 C and a long taper time of 2 h, the IR drop during the charge and discharge should be sufficiently small. Consequently, we may neglect the capacity measurement error originated from calculating the charge/discharge current by using the nominal capacity rather than the actual capacities with different taper voltages. Table 2 summarizes the capacities obtained from Fig. 9.

Next, we evaluated the effect of taper voltage on the current at the end of charge and the voltage at the end of discharge. We subjected the cells to five charge–discharge cycles at every taper voltage. Generally, the cell cycling behavior became stable after four cycles. Fig. 10 shows the current curves

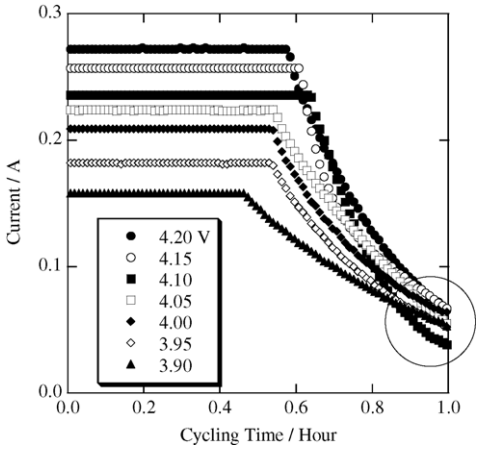

Fig. 10. Current-time charge curves at cycle 4 of every taper voltage for the lithium-ion polymer cell 5.

Table 2
Discharge capacity as a function of taper voltage

Taper voltage (V)	4.2	4.15	4.1	4.05	4.0	3.95	3.9
Discharge capacity (Ah)	0.549	0.517	0.477	0.451	0.420	0.366	0.320

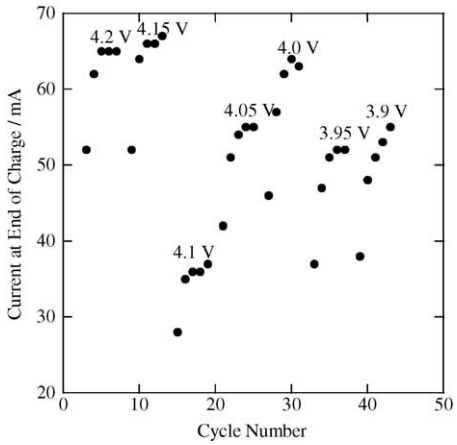

Fig. 11. Current at end of charge as a function of taper voltage for lithium-ion polymer cell 5 obtained from Fig. 10. The minimum current at end of charge was observed when using taper voltage of 4.10 V.

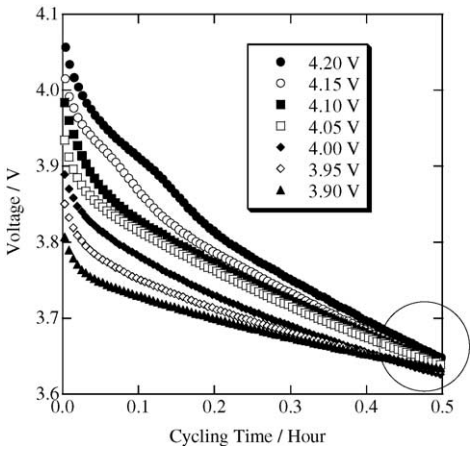

Fig. 12. Voltage–time discharge curves at cycle 4 of every taper voltage for the lithium-ion polymer cell 5.

of the charge phase at cycle 4 of every taper voltage. Basically, the time in the CC phase should decrease with decreasing taper voltage due to the decreasing capacity. Nevertheless, we found that the cell exhibited an exceptionally long time in the CC phase at a taper voltage of 4.10 V.

Fig. 10 reveals that the current performance in the CV phase depended extensively on the applied taper voltage. In order to interpret this correlation, Fig. 11 summarizes the current at the end of the charge as a function of taper voltage. Obviously, the current was minimum at the end of the charge when a taper voltage of 4.10 V was used, which was well consistent with the taper voltage where the time in the CC phase was exceptionally long. The current at the end of the charge decreased to 36 mA for a taper voltage of 4.10 V, compared to the maximum current of 66 mA. This indicated the significance of optimizing the taper voltage to improve the current performance.

The voltage at the end of the discharge is another important parameter reflecting the cycling performance. Fig. 12 presents the voltage curves of discharge phase at cycle 4 of every taper voltage. Obviously, the voltage curves exhibited very different profiles as a function of taper voltage. Since voltage at the beginning of the discharge decreased with taper voltage, it was naturally expected that the voltage at the end of discharge should have the same tendency. However, we found an exception in Fig. 13, which summarizes the voltage at the end of the discharge at every taper voltage. At the taper voltages of 4.10 and 405 V, the voltage at the end of discharge exceeded that at a taper voltage of 4.15 V. This indicated that 4.10 V and 405 V are the appropriate taper voltages at which a lithium-ion polymer cell exhibits both small current at the end of the charge and high voltage at the end of the discharge.

In a general sense, the applied voltage, V_{app}, for a lithium-ion cell must equal the sum of the open-circuit voltage, V_{OC}, the voltage drop due to the concentration polarization in electrode and electrolyte, V_{con}, and the voltage drop induced by the cell internal impedance, R.

$$V_{app} = V_{OC} + V_{con} + IR \quad (1)$$

Here I denotes the current.

If we assume that the current is enough small, then the lithium-ion diffusion becomes very slow in both electrolyte and electrode. As a result, the concentration polarization, and

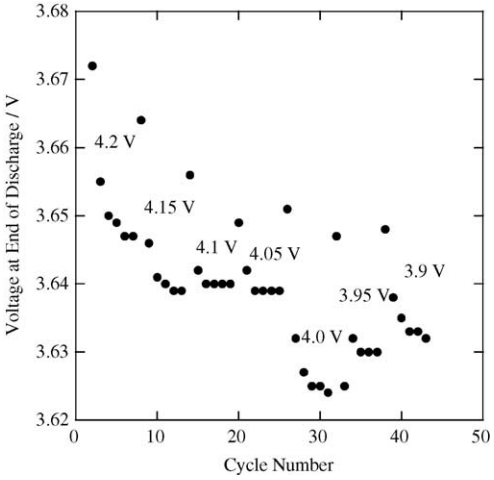

Fig. 13. Voltage at end of discharge as a function of taper voltage for the lithium-ion polymer cell 5 obtained from Fig. 12. An exceptionally high voltage was observed at end of discharge when using taper voltages of 4.10 and 4.05 V.

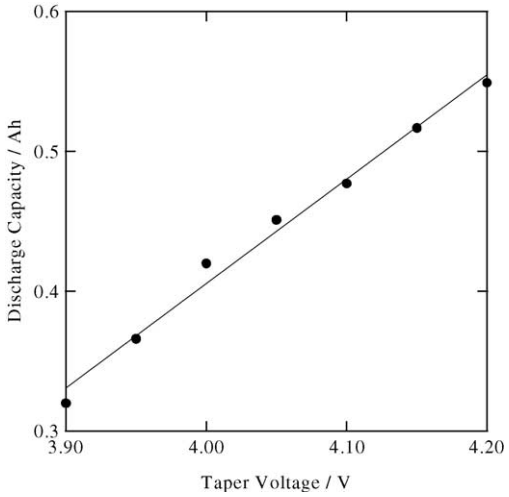

Fig. 14. Discharge capacity vs. taper voltage obtained from the data in Table 2. A linear relationship is observed.

hence V_{con}, decreased significantly, and may be ignored.

$$V_{con} = 0 \tag{2}$$

Replacing Eq. (1) by Eq. (2) yields

$$V_{app} = V_{OC} + IR \tag{3}$$

Eq. (3) may be rearranged as follows:

$$I = \frac{V_{app} - V_{OC}}{R} \tag{4}$$

In a charge condition of constant applied voltage, the change of current is represented by the change of open-circuit voltage.

$$\Delta I = -\frac{\Delta V_{OC}}{R} \tag{5}$$

Noting that $I = \Delta Q/\Delta t$ and rearranging yields

$$\frac{dI}{dt} = I\left[-\left(\frac{\Delta V_{OC}}{\Delta Q}\right)\left(\frac{1}{R}\right)\right] \tag{6}$$

where Q denotes the charge quantity, and t the time.

Using the current I_c, which is the initial value at the beginning of constant applied voltage, Eq. (6) may be integrated into Eq. (7) on condition that $\Delta V_{OC}/\Delta Q$ and R are constant.

$$I = I_c \exp\left\{\left[-\left(\frac{\Delta V_{OC}}{\Delta Q}\right)\left(\frac{1}{R}\right)\right]t\right\} \tag{7}$$

In a high charge rate, lithium-ion cell has a low R, which is almost constant. Therefore, whether $\Delta V_{OC}/\Delta Q$ is a constant becomes very important to secure the validity of Eq. (7).

In order to investigate this relationship, we plotted discharge capacity as a function of taper voltage, ΔV_{Taper}, based on the data of Table 2, as shown in Fig. 14. A linear relationship was observed, indicating that $\Delta V_{Taper}/\Delta Q$ was a constant. In the case that the charge rate is enough small, V_{Taper} should be equal to V_{OC}. This suggests that $\Delta V_{OC}/\Delta Q$ was also a constant and Eq. (7) is validity when charge rate is enough slow.

Since the change of charge quantity against the change of applied voltage, $\Delta Q/\Delta V$, has the same unit as a capacitor, Eq. (7) is formally similar to the current relationship of an resistance–capacitance (RC) circuit, which may be found in general electrochemical textbook [32].

We can draw two conclusions from Eq. (7). First, low cell internal impedance may lead to a small current at a given time. Next, current will be low at a given time if the change of open-circuit voltage against the change of charge quantity, $\Delta V_{OC}/\Delta Q$, is large. For low rate charging and discharging, the applied voltage, V_{app}, is approximately equal to the open-circuit voltage, $V_{OC,}$ according to Eq. (3). We can therefore use charge curves measured at a low rate to predict the optimum taper voltage at which the current at the end of the charge is minimum.

To examine the above, we plot example of charge and discharge curves of the lithium-ion polymer cell obtained at a low rate of 0.1 C in Fig. 15(a). Fig. 15(b) presents an enlarged charge curve with the voltage ranging from 3.9 to 4.2 V. The charge curve slope, $\Delta V/\Delta Q$, was maximum at a voltage of 4.05–4.10 V. In other words, if we take the taper voltage in

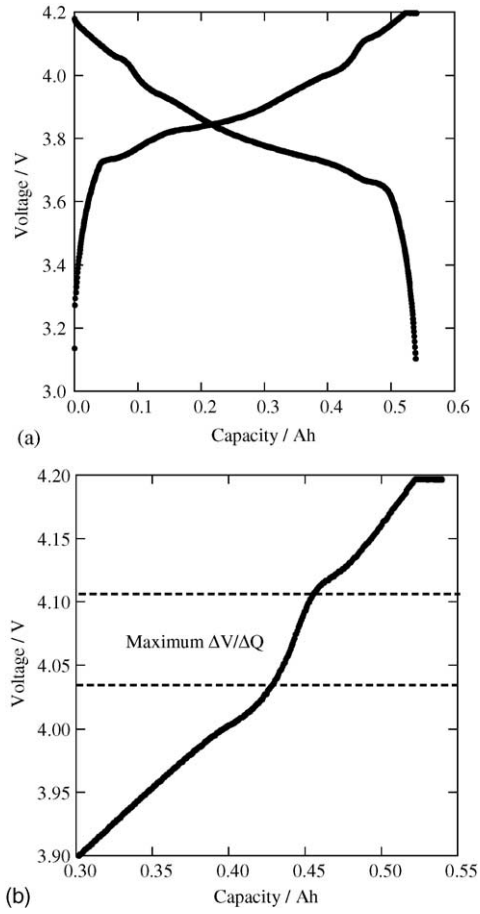

Fig. 15. (a) Charge and discharge curves and (b) enlarged charge curves for lithium-ion cell 5 measured at a low rate of 0.1 C. The maximum charge curve slope was observed at voltages ranging from 4.05 to 4.10 V.

this voltage range, the current at the end of the charge should be minimum. This agreed well with the experimental result obtained in Fig. 11 that 4.10 V is the most suitable taper voltage for minimizing the current at the end of the charge.

For a lithium-ion cell, the charge at the anode is generally designed to exceed that of the cathode. Consequently, cell-performance is mainly determined by the cathode. Some authors have reported that a $LiCoO_2$ cathode has a smaller lithium-ion diffusion coefficient in the two-phase coexistence region, which corresponds to a voltage plateau in charge and discharge curves [33,34]. In other words, if we take the voltage, where the slope ($\Delta V/\Delta Q$) is large in the charge curve, as the taper voltage, a lithium-ion cell should have large lithium-ion diffusion coefficient. This may be the main reason that a voltage range from 4.05 to 4.10 V was the important taper voltage where the cell had minimum current at the end of the charge and the lowest voltage at the end of the discharge.

Reviewing the above results and discussion reveals that the taper voltage is an important operation condition for lithium-ion cells used as satellite power sources. An appropriate taper voltage, which falls into the voltage range where the change of applied voltage against the change of charge quantity is maximum in a slow-rate charge curve, may considerably improve cell cycle-life performance. One major problem causing capacity fading of a lithium-ion cell is redox decomposition of electrolyte and contaminates at high voltage in which products are deposited on the electrode surface and increase cell internal impedance. For this reason, selecting a lower taper voltage in the above voltage range is important for improving cycle-life performance in initial charge–discharge cycles. Nevertheless, cell internal impedance generally increases with cycling and hence leads to increased cell-voltage drop, *IR*. Consequently, cell voltage, V_{OC}, became smaller and smaller for a constant applied voltage, V_{app}, according to Eq. (3). This results in capacity fading of a cell due to a lower cell voltage than the setup value. Therefore, appropriately increasing taper voltage may be an effective approach to extending cell life when the cell-voltage drop ultimately affects satellite operation.

4. Conclusions

In order to develop lithium-ion polymer batteries for space applications, we assessed the effect of operation conditions, charge rate and taper voltage, on cycle-life testing of commercial lithium-ion polymer cells by simulating a satellite's LEO operation with 40% DOD profile at room temperature.

So far, 6000 cycles have been completed, corresponding to 1 year of LEO satellite operation. During initial cycles, a high charge rate led to good cycling performance, such as low current at the end of the charge and similar voltage at the end of the discharge. Nevertheless, with cycling, the voltage at the end of the discharge declined severely at high charge rates. After 3000 cycles, the voltage at the end of the discharge with a high charge rate became lower than that with a low charge rate. An impedance analysis indicated that the poor cycling performance at a high charge rate was attributed to excessive lithium-ion exhaust in electrode surface-film formation due to a longer holding duration at taper voltage, rather than cell-internal-impedance increase.

Short-term cycle-life testing simulating a LEO satellite application disclosed that taper voltage affected charge performance of lithium-ion polymer cells. The minimum current at the end of the charge and the maximum voltage at the end of the discharge were observed when using taper voltage range from 4.05 to 4.10 V. To interpret these experimental results, we theoretically analyzed a lithium-ion cell and deduced that low current at the end of the charge correlated to (1) low cell internal impedance and (2) a large slope in the capacity–voltage charge curve measured at a low rate. We further evaluated cell cycling behavior at a low rate and observed the largest slope of capacity–voltage charge curve at voltages ranging from 4.0 to 4.1 V. This agreed well with the experimental result that 4.05 and 4.10 V were the appropriate taper voltages, where the cell exhibited good cycling performance.

Acknowledgments

Japan Aerospace Exploration Agency (JAXA) assisted in meeting the publication costs of this article.

References

[1] J.K. McDermott, in: J.R. Wertz, W.J. Larson (Eds.), Space Mission Analysis and Design, 3rd ed., The Space Technology Library, California, 1999, p. 407.
[2] P. Cowles, D. Lizius, R. Spurett, C. Thwaite, M. Slimm, in: Proceedings of the 18th AIAA International Communication Satellite Systems Conference and Exhibit, AIAA, Oakland, USA, 2000.
[3] G. Gave, Y. Borthomieu, B. Lagattu, J.P. Planchat, in: Proceedings of the 51st International Astronautical Congress, International Astronautical Federation, Rio de Janeiro, Brazil, 2000.
[4] Y. Borthomieu, in: Proceedings of the 1999 NASA Aerospace Battery Workshop (CD-ROM Version), Marshall Space Flight Center, Huntsville, USA, 2000.
[5] T. Inoue, T. Sasaki, N. Imamura, H. Yoshida, M. Mizutani, in: Proceedings of the 2001 NASA Aerospace Battery Workshop (CD-ROM Version), Marshall Space Flight Center, Huntsville, USA, 2002.
[6] S. Kuwajima, in: Yuichi Sato (Ed.), Battery Technology, The Committee of Battery Technology, The Electrochemical Society of Japan, Tokyo, 2002, vol. 14.
[7] Y. Sone, X. Liu, H. Kusawake, K. Kanno, S. Kuwajima, in: Proceedings of the 2000 NASA Aerospace Battery Workshop (CD-ROM Version), Marshall Space Flight Center, Huntsville, USA, 2001.
[8] Y. Sone, X. Wang, H. Kusawake, K. Kanno, S. Kuwajima, Marshall Space Flight Center, Huntsville, USA in: Proceedings of the 2002 NASA Aerospace Battery Workshop (CD-ROM Version), 2003.
[9] X. Wang, Y. Sone, H. Kusawake, K. Kanno, S. Kuwajima, in: Proceedings of the 2002 NASA Aerospace Battery Workshop (CD-ROM Version), Marshall Space Flight Center, Huntsville, USA, 2003.
[10] G. Bruce, P. Mardikian, L. Macoux, in: Proceedings of the Fifth European Space Power Conference ESA SP-416, Tarragona, Spain, 1998, p. 481.

[11] R. Spurrett, M. Slimm, C. Thwaite, in: Proceedings of the Fifth European Space Power Conference ESA SP-416, Tarragona, Spain, 1998, p. 475.
[12] B.V. Ratnakumar, M.C. Smart, A. Kindle, H. Frank, R. Ewell, S. Surampudi, J. Power Sources 119–121 (2003) 906.
[13] J.P. Fellner, G.J. Loeber, S.P. Vukson, C.A. Riepenhoff, J. Power Sources 119–121 (2003) 911.
[14] Y. Borthomieu, in: Proceedings of the 1999 NASA Aerospace Battery Workshop (CD-ROM Version), Marshall Space Flight Center, Huntsville, USA, 2000.
[15] J. Baker, P. Shah, G. Nagasubramanian, D. Doughty, in: S. Surampudi, R.A. Marsh, Z. Ogumi, J. Prakash (Eds.), Lithium Batteries: Proceedings of the International Symposium, PV 99-25, The Electrochemical Society Proceedings Series, Pennington, NJ, 1999, p. 664.
[16] G.J. S Dudley, in: Proceedings of the Fifth European Space Power Conference ESA SP-416, Tarragona, Spain, 1998, p. 17.
[17] M.C. Smart, B.V. Ratnakumar, S. Surampudi, J. Electrochem. Soc. 146 (1999) 486.
[18] C. Picart, P. Willmann, B. Castets, G. Buat-Menard, in: Proceedings of the Fifth European Space Power Conference ESA SP-416, Tarragona, Spain, 1998, p. 487.
[19] P. Johnson, C. Lurie, R. Spurrett, in: Proceedings of the 2001 NASA Aerospace Battery Workshop (CD-ROM Version), Marshall Space Flight Center, Huntsville, USA, 2002.
[20] M. Schautz, D. Olsson, G. Dudley, A. Holland, in: Proceedings of the 2001 NASA Aerospace Battery Workshop (CD-ROM Version), Marshall Space Flight Center, Huntsville, USA, 2002.
[21] Y. Chang, H. Sohn, J. Electrochem. Soc. 147 (2000) 50.
[22] M. Doyle, J.P. Meyers, J. Newman, J. Electrochem. Soc. 147 (2000) 99.
[23] K. Sawai, T. Ohzuku, J. Electrochem. Soc. 150 (2003) 674.
[24] B.A. Johnson, R.E. White, J. Power Sources 70 (1998) 48.
[25] J. Baker, R. Pynenburg, R. Koksbang, M.Y. Saidi, Electrochim. Acta 41 (1996) 2481.
[26] D. Zhang, B.N. Popov, B.S. Haran, R.E. White, Y.M. Podazhansky, in: S. Surampudi, R.A. Marsh, Z. Ogumi, J. Prakash (Eds.), Lithium Batteries: Proceedings of the International Symposium, PV 99-25, The Electrochemical Society Proceedings Series, Pennington, NJ, 1999, p. 645.
[27] M. Doll, F. Orsini, A.S. Gozdz, J.-M. Tarascon, J. Electrochem. Soc. 148 (2001) 851.
[28] J.R. Dahn, A.K. Sleigh, H. Shi, B.M. Way, W.J. Weydanz, J.N. Reimers, Q. Zhong, U. von Sacken, in: G. Pistoia (Ed.), Lithium Batteries: New Materials, Developments, and Perspectives, Elsevier, Amsterdam, 1994.
[29] E. Endo, K. Tanaka, K. Sekai, J. Electrochem. Soc. 147 (2000) 4029.
[30] C. Lee, B. Mun, P.N. Ross, J. Electrochem. Soc. 149 (2002) 1286.
[31] X. Wang, Y. Sone, S. Kuwajima, J. Electrochem. Soc. 151 (2004) 273.
[32] A.J. Bard, L.R. Faulkner, Electrochemical Methods, in: Fundamentals and Applications, 2nd ed., Wiley, New York, 2001.
[33] K. Dokko, S. Horikoshi, M. Nishizawa, T. Itoh, T. Abe, I. Uchida, in: S. Surampudi, R.A. Marsh, Z. Ogumi, J. Prakash (Eds.), Lithium Batteries: Proceedings of the International Symposium, PV 99-25, The Electrochemical Society Proceedings Series, Pennington, NJ, 1999, p. 290.
[34] M.D. Levi, G. Salitra, B. Markovsky, H. Teller, D. Aurbach, U. Heider, L. Heider, J. Electrochem. Soc. 146 (1999) 1279.